Bol. Soc. Paran. Mat.
©SPM – E-ISSN-2175-1188
SPM: www.spm.uem.br/bspm

(3s.) **v. 2026 (44) 16** : 1–19.
ISSN-0037-8712
doi:10.5269/bspm.81988

Impacts of Magneto-Hydrodynamics and Slip Velocity Effects on Curved Circular and Porous- Rough Flat Plate Lubricated with Couple Stress Fluid

Shivaraj M. Dandoti, Jagadish Patil, Bannihalli Naganagowda Hanumagowda and Suvarna Hindole

ABSTRACT: This paper presents a theoretical analysis of the influence of slip velocity and couple stress on the squeeze film lubrication of curved circular and flat plates with a rough and porous lower plate and an externally supplied magnetic field. The space between the plates is filled by a conductive non-Newtonian lubricant layer with nominal rough and smooth sections. The modified Reynolds equation is derived from Christensen's stochastic theory of rough surfaces, and the Darcy law is applied to porous mediums. Expressions for dimensionless pressure distribution, load bearing capacity, and squeeze film time are obtained. The revised Reynolds equation is solved, and the results are presented in terms of squeezing film bearing qualities for various physical factors, with graphs displayed. Surface roughness effects are especially pronounced in couple stress lubricants with transverse magnetic fields and slip velocity. The roughness parameter, capability of carrying load and time of squeeze film rises in the Azimuthal roughness case, while these quantities decrease in the Radial roughness case. Permeability also results in a decrease in the capability of carrying load and response time when compared to the impermeable cases.

Keywords: MHD, slip velocity, Porous-Rough, curved flat late, couple stress, Reynolds's equation.

Contents

1. Introduction

Magneto hydrodynamic (MHD) bearings provide a stabilizing Lorentz force by combining magnetic fields with electrically conducting fluids. By using conductive fluids, including liquid metals or electrolytes, in place of conventional lubricants and applying magnetic fields via electromagnets or permanent magnets, these bearings lessen mechanical contact. Reduced wear and friction, increased load carrying capacity, precise control by magnetic field adjustment, and suitability for harsh environments are some benefits of MHD bearings. MHD bearings provide novel solutions in cutting-edge engineering applications by combining fluid mechanics, electromagnetic, and materials science in a state-of-the-art manner. For wider usage, however, issues with energy efficiency and material design must be resolved. Kuzma [1] applied the MHD idea to journal bearings. The study sought to determine how using a magnetic field and conductive lubricant may improve journal bearing performance. Understanding how hydrodynamic forces and electromagnetic effects interact in the bearing system was the main goal. Kuzma work established the groundwork for the creation of MHD bearings and stimulated more study into the use of electromagnetics in lubrication systems. This work is a pioneer in the use of electromagnetic and fluid dynamics to engineering challenges. According to Krieger et al. [2] study, MHD Hydrostatic Thrust Bearing-Theory and Experiments, experimental results support the models and show that MHD effects improve bearing performance. Draw attention to issues with practical use, such sustaining consistent magnetic fields. Journal bearings [3] by Kamiayama Moreover, Lin [5] and Malik and Singh [4]

2020 *Mathematics Subject Classification:* 76W05, 76A05, 76D08, 76D99.
Submitted February 14, 2026. Published May 02, 2026.

examined the MHD stable and dynamic properties of broad tapered-land slider bearings. These authors noted that MHD lubrication may be advantageous for increased stability and decreased friction in high-speed applications. Couple stress fluids are a class of non-Newtonian fluid with microstructural characteristics including body couples and size-dependent properties not well explained by traditional fluid models. These fluids address rotating interactions between particles and are clarified using ideas extending classical continuum mechanics. Couple stress effects give the fluid film more resistance through microstructural interactions, hence improving its load-carrying capacity. In couple stress fluids, micro-rotational effects lower friction, enhance bearing performance, and slow down wear. High-performance lubricants, particularly in challenging situations requiring exact control of friction and wear, like aircraft bearings, high-speed equipment, nano and micro-mechanical systems, find use for couple stress fluids. Lin [6] provided the MHD couple stress on curved circular squeeze film bearings using non-Newtonian fluid on finite journal bearings; Dynamically loaded bearing by Wang et al [7], rough slider bearings by Naduvinamani [8], Lin et al. [9]] presented By Crosby and Chetti [10,11], dynamic and static aspects of a two-lobe journal bearing include preload effects on the static properties of three-lobe journal bearings. These values highlight the value of couple-stress fluids in enhancing the performance of bearings concerning both static and dynamic properties. They also draw attention to the possibility for optimization by means of preload and lobe geometry in design terms. Combining Couple Stress Fluid theory with Magneto hydrodynamics (MHD) presents a strong framework for evaluating and maximizing bearing performance under challenging operational environments. While also considering the microstructural impacts of couple stress fluids, bearings running with an MHD couple stress lubricant use electrically conducting fluids impacted by magnetic fields. Advances in metallurgy and lubrication technology have helped to define porous bearings, sometimes referred to as sintered or self-lubricating bearings. The idea of porous bearings first surfaced in the early 1900s when powdered metallurgy developed. By compressing and heating metal powders, the sintering technique made it possible to produce porous structures able of containing lubricants. Early uses for low-maintenance bearings in machinery running under demanding conditions, such textile and agricultural equipment, motivated early applications. These days, porous bearing are standard in many different sectors, including industrial machinery, aircraft, and automotive. Improving their performance under extreme conditions—such as high temperatures, corrosive environments, and zero-gravity applications—is the main emphasis of continuous study. Using wide composite slider porous bearings, Kashinath and Hanumagowda [12] conducted analysis showing the possibility of combining MHD and couple stress fluids to improve bearing performance, especially in applications needing high load capacity and low friction. These results are pertinent in sectors including aircraft, automotive, and power generation where sophisticated lubricating methods are vital. Showing the exponential porous bearings with MHD-couple stress lubricants, Naduvinamani and Shridevi [13] Particularly suited for enhancing pressure distribution, the study makes use of an exponential slider bearing model with a non-linear film thickness distribution. We study how lubricant flow via the porous structure influences the load capacity, and film thickness by modeling porosity. Jagadish Patil et al [14] have investigated the porosity influence on curved circular an open plate. Furthermore, Hiremath et al. [15] investigated flat and curved circular plate with MHD couple stress fluid. Umadevi et al. [16] reported pair stress fluid and MHD slip velocity analysis. Author claimed that the bearings suffered depending on the permeability parameter. Bearing performance depends much on surface roughness since it directly influences the lubrication regime, friction, wear, and general efficiency. Bearings are meant to minimize friction and assist loads. Materials and coatings with diamond-like carbon (DLC) or ceramics help to reduce the negative impacts of roughness and improve bearing life. Author Christensen [17] investigated Stochastic model hydrodynamic rough surfaces and noted the effect of roughness. On spherical bearing, roughness impact was Gupta and Daheri [18] Vijayalxmi et al. [19]] lately addressed the roughness between curved circular and flat plate. Author claimed that the enhanced bearing performance results from using MHD couple stress with increasing slip velocity. MHD slip velocity effect on conical and SCAC plates Ramesh et al., [20,21]. The consequence of porous-roughness on curved circular flat plates of porous roughness, in combination with applied magnetic fields and slip velocity not yet investigated by any researchers. Jayaprakash et al. [22] this study investigates the theoretical impact of MHD on curved circular and plane plates using non-Newtonian lubricants. The lower plate is porous, and the research focuses on understanding how MHD influences the lubrication characteristics in such configurations. Byeon et al. [23]

The authors analyse the influence of surface roughness, MHD, and viscosity variation on the couple stress squeeze film characteristics between curved circular and flat plates. They employ Christensen's stochastic theory for rough surfaces to assess parameters like pressure, load-carrying capacity, and squeeze film time across various physical conditions. Shah [24] This research examines the effects of porous-roughness on different circular disc squeeze film bearing designs lubricated with ferrofluids. By deriving a modified stochastic Reynolds–Darcy equation under a variable magnetic field, the study compares performances of various bearing designs, highlighting the significance of factors like circumferential roughness and disc curvature. Thus, this work intends to investigate using a non-Newtonian fluid effect of porous roughness along slip velocity and MHD on these plates. Darcy's rule for porous media generates a modified Reynolds equation; Christensen's Stochastic theory is then used to explain surface roughness. Moreover, obtained the expressions for distribution of pressure, load-bearing capability, and film squeezing time.

2. Mathematical Formulation of the Model

Figure 1; shows the bearing system model, which includes two types of plates: circular and flat with porous- rough, parted by a film thickness h. The bottom layer is thought to have a rough surface and a porous of thickness δ. The bottom plate remains motionless while the upper plate is in motion toward the bottom plate at a speed of V. A uniform magneitc field B0 is applied perpendicular to the Z- direction. Here we have a thin layer of fluid with low inertia, little induced magnetic field relative to applied magnetic field, and almost no body force other than the Lorentz force.

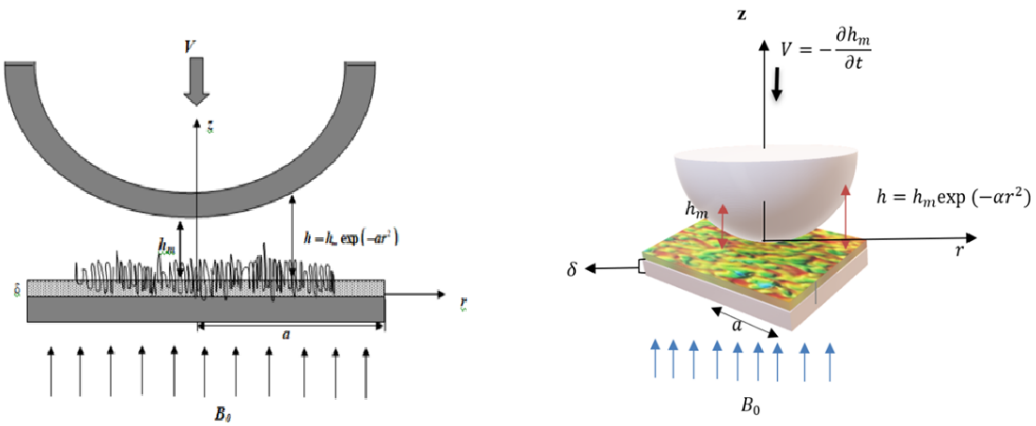

(a) Geometry of the problem

(b) 3D model of the problem.

Figure 1: Geometry and 3D model of the problem

A film width is separated into two categories:

$$H = h + h_s(r, z, \xi) \tag{2.1}$$

Where, $h = \exp(-\alpha r^2)h_m$, $0 \leq r \leq a$ denote thickness of the fluid film and $h_s(r, z, \xi)$ is rough structure, h_m be a minimum film thickness. Following these predictions, considering the basic governing equations as

$$\mu \frac{\partial^2 u}{\partial z^2} - \eta \frac{\partial^4 u}{\partial z^4} - \sigma B_0^2 u = \frac{\partial p}{\partial r} \tag{2.2}$$

$$\frac{\partial p}{\partial z} = 0 \tag{2.3}$$

$$\frac{1}{r}\frac{\partial}{\partial r}(ru) + \frac{\partial w}{\partial z} = 0 \tag{2.4}$$

Where, u, v velocities along r and θ paths, pressure p in film section, η is the new material constant for non-Newtonian fluid, μ is dynamic viscosity and σ electrical conductivity. For the porous region

$$\frac{\partial w^*}{\partial z} + \frac{\partial u^*}{\partial r} = 0 \tag{2.5}$$

Where, velocity components u^* and w^* from the Darcy's law,

$$u^* = \frac{-k}{\left(1 - \phi + \dfrac{kM^2}{mh_m^2}\right)\mu} \frac{\partial p^*}{\partial r} \tag{2.6}$$

$$w^* = \left(\frac{-k}{\mu(1-\phi)}\right) \frac{\partial p^*}{\partial z} \tag{2.7}$$

Where,$\phi = \frac{(\eta/\mu)}{k}]$ represents the microstructure relation of size to pore size, m is porosity, and k permeability of porous region. The applicable boundary circumstances are:

i) Upper plate height $z = h$

$$u = 0, \qquad \frac{\partial^2 u}{\partial z^2} = 0, \qquad v = -\frac{\partial h_m}{\partial t} \tag{2.8}$$

ii) Lower plate height $z = 0$

$$u = \frac{1}{s}\left(\frac{\partial u}{\partial z}\right)_{z=0}, \qquad \frac{\partial^2 u}{\partial z^2} = 0, \qquad v = 0 \tag{2.9}$$

$$s = \frac{\alpha}{\sqrt{k}} \tag{2.10}$$

Where, s is slip velocity.

The velocity component u is obtained by solving eqn.(2.2) utilising (2.8), (2.9) we get

$$u = \left[\frac{1}{\phi_2} \times \phi_3 - \phi_4 - 1\right] \frac{h_m^2}{\mu M^2} \frac{\partial p}{\partial r} \tag{2.11}$$

Where,

$$\phi_1 = 1 - \frac{AB^2}{(A^2 - B^2)s\,l}\left(\operatorname{cosech}\frac{Ah}{l}\right) + \frac{BA^2}{(A^2 - B^2)s\,l}\left(\operatorname{cosech}\frac{Bh}{l}\right),$$

$$\phi_2 = 1 - \frac{AB^2}{(A^2 - B^2)s\,l}\coth\frac{Ah}{l} - \frac{BA^2}{(A^2 - B^2)s\,l}\coth\frac{Bh}{l}$$

$$\phi_3 = \frac{A^2}{(A^2 - B^2)}\frac{\sinh\left(\dfrac{B(z-h)}{l}\right)}{\sinh\left(\dfrac{Bh}{l}\right)} + \frac{B^2}{(A^2 - B^2)}\frac{\sinh\left(\dfrac{A(z-h)}{l}\right)}{\sinh\left(\dfrac{Ah}{l}\right)}$$

and

$$\phi_4 = \frac{1}{(A^2 - B^2)}\left[A^2 \sinh\frac{Az}{l}\operatorname{cosech}\frac{Ah}{l} - B^2 \sinh\frac{Bz}{l}\operatorname{cosech}\frac{Bh}{l}\right]$$

The Reynolds equation is obtained by substituting the boundary conditions (2.5), (2.6), and (2.7) into equation (2.4) and then performing an integration across the film thickness.

$$-\left(V - v\big|_{h=h_0}\right) = \frac{1}{r}\frac{\partial}{\partial r}\left\{-\frac{r}{\mu}\frac{\partial p}{\partial r} f(h, l, s, B_0)\right\} \tag{2.12}$$

$$f(B_0, h, l, s) = \frac{l}{(A^2 - B^2)}\left(\frac{2 - \xi_1 \coth\frac{Ah}{l} + \xi_2 \coth\frac{Bh}{l}}{1 - \xi_1 \coth\frac{Ah}{l} + \xi_2 \coth\frac{Bh}{l}}\right)\left\{\left[\frac{B^2}{A}\tanh\left(\frac{Bh}{2l}\right) - \frac{A^2}{B}\tanh\left(\frac{Bh}{2l}\right)\right] + \frac{(A^2 - B^2)}{l}\right\}\frac{1}{\sigma B_0^2}$$

$$\xi_1 = \frac{AB^2}{(A^2-B^2)s\,l}, \qquad \xi_2 = \frac{A^2B}{(A^2-B^2)s\,l}$$

$$A = \left[\frac{1+\sqrt{1-4M_0^2l^2/h_m^2}}{2}\right]^{1/2}, \qquad B = \left[\frac{1-\sqrt{1-4M_0^2l^2/h_m^2}}{2}\right]^{1/2}$$

Since upper plate is no porous $w_h = 0$.
At the interface with the bottom plate, the z-component of velocity remains continuous.

$$v\big|_{z=0} = \frac{k}{\mu(1-\phi)}\left(\frac{\partial p^*}{\partial z}\right)_{z=0} \tag{2.13}$$

Substituting (2.13) in (2.12) we get modified form of Reynolds equation

$$\frac{1}{r}\frac{\partial}{\partial r}\left[\frac{r}{\mu}\frac{\partial p}{\partial r}f(h,l,s,B_0)\right] = V + \frac{k}{\mu(1-\phi)}\left(\frac{\partial p^*}{\partial z}\right)_{z=0} \tag{2.14}$$

Within the porous region, the fluid pressure fulfils the equation

$$r\frac{\partial p^*}{\partial r}\frac{1}{r}\frac{\partial}{\partial r} + \frac{D}{(1-\phi)}\frac{\partial^2 p^*}{\partial z^2} = 0$$

Where,

$$D = \left[1-\phi+\frac{kM^2}{mh_m^2}\right]$$

By utilizing BC, we integrate the equation above concerning z throughout the thickness δ of the porous sheet of the solid:

$$\frac{\partial p^*}{\partial r} = 0 \quad \text{at } z = -\delta$$

$$\left(\frac{\partial p^*}{\partial z}\right)_{z=0} = -\frac{1-\phi}{D}\int_{-\delta}^{0}\frac{1}{r}\frac{\partial}{\partial r}\left(r\frac{\partial p^*}{\partial r}\right)dz \tag{2.15}$$

Predicting δ is very less and backing conditions $p = p^*$ at porous interface $z = 0$,

$$\left(\frac{\partial p^*}{\partial z}\right)_{z=0} = -\delta\left(\frac{1-\phi}{D}\right)\frac{1}{r}\frac{\partial}{\partial r}\left(r\frac{\partial p}{\partial r}\right) \tag{2.16}$$

Using Eq.(2.16) in Eq.(2.14).

$$\frac{1}{r}\frac{\partial}{\partial r}\left[\left(f(B_0,h,l,s)+\frac{\delta k}{D}\right)r\frac{\partial E(p)}{\partial r}\right] = V\mu \tag{2.17}$$

This stochastic model separates the film thickness in two components and generates the information suitable for surface roughness analysis.

$$H = h + h_s(r,z,\xi) \tag{2.18}$$

ξ stands for the index parameter that establishes a particular roughness pattern. Many engineering challenges have surfaces with roughness height distributions that are Gaussian. We provide a near-Gaussian approximation for this class of probability density functions.

$$f(h_s) = \begin{cases} \frac{35}{32C^7}(c^2-h_s^2)^3, & -c < h_s < c, \\ 0, & \text{elsewhere.} \end{cases}$$

Where, $\overline{\sigma}$ is the S.D., $C = 3\overline{\sigma}$. Let h_s is thickness of the stochastic film.
The stochastic mean of (2.17) w.r.t. $f(h_s)$ modified Reynolds expression is calculated as

$$\frac{1}{r}\frac{\partial}{\partial r}\left[rE\big(f(B_0,H,l,s)\big)\frac{\partial E(p)}{\partial r}\right] = \mu V \tag{2.19}$$

Here, $E(\bullet)$ stands for the expectation operator as described by

$$E(\bullet) = \int_{-\infty}^{\infty} (\bullet)\, f(h_s)\, dh_s$$

Radial roughness: Surfaces characterized by long, narrow ridges and valleys aligned in the r-direction create one-dimensional radial roughness patterns. The film thickness is expressed as:

$$H = h + h_s(r,\xi) \tag{2.20}$$

The modified stochastic Reynolds equation (2.19) is

$$\frac{1}{r}\frac{\partial}{\partial r}\left[rE\left(\frac{\delta k}{D} + f(B_0,H,l,s)\right)\frac{\partial E(p)}{\partial r}\right] = \mu V \tag{2.21}$$

Azimuthal roughness: The 1–D Azimuthal surface roughness, which shows long, thin ridges and a z-direction valley, determines film thickness.

$$H = h + h_s(z,\xi) \tag{2.22}$$

$$\frac{1}{r}\frac{\partial}{\partial r}\left[\left(\frac{1}{E\big(f(B_0,H,l,s)\big)} + \frac{\delta k}{D}\right) r\frac{\partial E(p)}{\partial r}\right] = \mu V \tag{2.23}$$

The following formula is obtained by combining equations (2.23) and (2.21):

$$\frac{1}{r}\frac{\partial}{\partial r}\left[\left(K(B_0,H,l,s,c) + \frac{\delta k}{D}\right) r\frac{\partial E(p)}{\partial r}\right] = \mu V \tag{2.24}$$

Where,

$$K(M_0,l,H,c) = \begin{cases} E\big(f(B_0,H,l,s)\big), & \text{Radial,} \\ \left[E\left(\dfrac{1}{f(B_0,H,l,s)}\right)\right]^{-1}, & \text{Azimuthal.} \end{cases} \tag{2.25}$$

$$E\big(f(H,l,B_0,s)\big) = \frac{35}{32c^7}\int_{-c}^{c} f(B_0,H,l,s)(c^2-h_s^2)^3\, dh_s \tag{2.26}$$

$$E\left(\frac{1}{f(B_0,H,l,s)}\right) = \frac{35}{32c^7}\int_{-c}^{c} \frac{(c^2-h_s^2)^3}{f(B_0,H,l,s)}\, dh_s \tag{2.27}$$

Introducing dimensionless quantities

$$r^* = \frac{r}{a}, \quad H^* = \frac{H}{h_m}, \quad h_0^* = \frac{h_0}{h_m}, \quad l^* = \frac{l}{h_m}, \quad K = \beta a^2, \quad C = \frac{c}{h_m}, \quad s^* = \frac{\sigma^*}{h_m},$$

$$P = \frac{h_m^3 p}{\mu a^2 V}, \quad \psi = \frac{k\delta}{h_m}, \quad D_1 = \left(1 - \phi + \frac{kM_0^2}{mh_m^2}\right), \quad h^* = \frac{h}{h_m} = \exp(-\alpha r^{*2}), \quad 0 \le r^* \le 1.$$

By substituting the given values into equation (2.24), the dimensionless modified Reynolds equation is obtained.

$$\frac{1}{r^*}\frac{\partial}{\partial r^*}\left[r^* F(M_0^*,l^*,H^*,s^*,C,\psi)\frac{\partial P}{\partial r^*}\right] = -1 \tag{2.28}$$

Where,

$$F^*(M_0, H^*l^*, s^*, C) = \frac{l^*}{(A^{*2} - B^{*2})M^2}\left\{\frac{\left[2 - \xi_1^* \coth\left(\frac{A^*H^*}{2l^*}\right) + \xi_2^* \coth\left(\frac{B^*H^*}{2l^*}\right)\right]}{\left[1 - \xi_1^* \coth\left(\frac{A^*H^*}{l^*}\right) + \xi_2^* \coth\left(\frac{B^*H^*}{l^*}\right)\right]}\right.$$
$$\times \left[\frac{B^{*2}}{A^*}\tanh\left(\frac{B^*H^*}{2l^*}\right) - \frac{A^{*2}}{B^*}\tanh\left(\frac{B^*H^*}{2l^*}\right)\right]$$
$$\left. + \frac{(A^{*2} - B^{*2})}{l^*}H^*\right\} + \frac{\psi}{D_1}$$

$$\xi_1^* = \frac{A^*B^{*2}}{(A^{*2} - B^{*2})s^*l^*}, \qquad \xi_2^* = \frac{B^*A^{*2}}{(A^{*2} - B^{*2})s^*l^*}$$

$$A^* = \sqrt{\frac{1 + \sqrt{1 - 4M_0^2l^{*2}}}{2}}, \qquad B^* = \sqrt{\frac{1 - \sqrt{1 - 4M_0^2l^{*2}}}{2}}$$

$$F(H^*, l^*, M_0, s^*, C, \psi) = \begin{cases} E(f(M, H_0^*, l^*, s^*)), & \text{Radial Roughness,} \\ \left[E\left(\frac{1}{f(M_0, H^*, l^*, s^*)}\right)\right]^{-1}, & \text{Azimuthal Roughness.} \end{cases}$$

Radial Roughness:

$$E(f^*(M_0, H^*, l^*, s^*)) = \frac{35}{32C^7}\int_{-C}^{C} f^*(M_0, H^*, l^*, s^*)(C^2 - h_s^{*2})^3\, dh_s^*$$

Azimuthal Roughness:

$$E\left(\frac{1}{f^*(M_0, H^*, l^*, s^*)}\right) = \frac{35}{32C^7}\int_{-C}^{C} \frac{(C^2 - h_s^{*2})^3}{f^*(M_0, H^*, l^*, s^*)}\, dh_s^*$$

Squeeze film pressure related boundary conditions are

$$\frac{dP}{dr^*} = 0 \quad \text{at} \quad r^* = 0 \tag{2.29}$$

$$P = 0 \quad \text{at} \quad r^* = 1 \tag{2.30}$$

To obtain the dimensionless squeeze film pressure, equation (2.28) is integrated with respect to the given variable while applying the boundary conditions (2.29) and (2.30).

$$P = -\frac{1}{2}\int_{r^*}^{1} \frac{r^*}{F(M_0, H^*, s^*, l^*, C, \psi)}\, dr^* \tag{2.31}$$

A dimensionless load bearing capacity may be obtained by integrating Equation (31) from 0 to 1.

$$W^* = -2\int_0^1 \left[\int_{r^*}^1 \frac{r^*}{F(M_0, H^*, s^*, l^*, C, \psi)}\, dr^*\right] r^*\, dr^* \tag{2.32}$$

Incorporating the minimal film thickness into the aforementioned calculation yields the dimensionless squeeze film time.

$$T^* = -2\int_0^1 \left[\int_0^1 \left(\int_{r^*}^1 \frac{r^*}{F(M_0, H^*, l^*, s^*, C, \psi)}\, dr^*\right) r^*\, dr^*\right] dh_s^* \tag{2.33}$$

Where,

$$h^* = h_m^* \exp(-Kr^{*2})$$

3. Result and Discussion

The behaviour of bearing characteristics such as pressure distribution, load capacity, and squeeze film time can be explained by the numerical solution of the modified Reynolds Equation. All required characteristic features of squeeze film bearings such as the pressure distribution, load-carrying capacity and squeezing time have been obtained as functions of dimensionless Hartmann number M_0, roughness parameter C, Permeability Parameter ψ, couple-stress parameter l^* and slip velocity s^* with the help of Stokes theory and Christensen's stochastic theory was carried out.Results are interpreted graphically where the dotted line represents azimuthal pattern and solid line is for radial pattern. In case of smooth surface ($C \to 0$) and absence of porosity ($\psi \to 0$)this study reduces to the investigation of Hiremath et al. [15]. In case of Slip velocity to zero ($s \to 0$)the current study reduces to the study of Jayaprakash et al [22].

3.1. Dimensionless Squeeze Film Pressure

Figure 2, indications the pressure P along r^*as influence of $C$and $s^*$for both roughness structures and found that for higher values C, pressure increases in the azimuthal roughness structure whereas, decrease found in the radial roughness when $C \to 0$referrers reduces in smooth case. In Figure 3, is P versus r^* for distinctive ψ is displayed and noted that pressure P decreases due to the impact of permeability parameter ψ, Figure 4, and 5,, for characteristic values of M_0 and couple stress parameter the graph P against r^* is offered and seen that the impact of M_0 and l^* is to enhance P. Figure 6, describes the P along r^* for distinctive values of slip velocity parameterss^*. However, the bearing surfaces roughness asperities also lower the fluids velocity. Additionally, the occurrence of surface asperities again diminishes the quantity of lubricant leaking along the sidewise direction. The area collects a lot of fluid overall, which creates a wide dispersion of pressure. These numbers make these disparities quite evident. Therefore, the non-Newtonian fluid, roughness, and magnetic field are advantageous elements for expanding the pressure distribution.

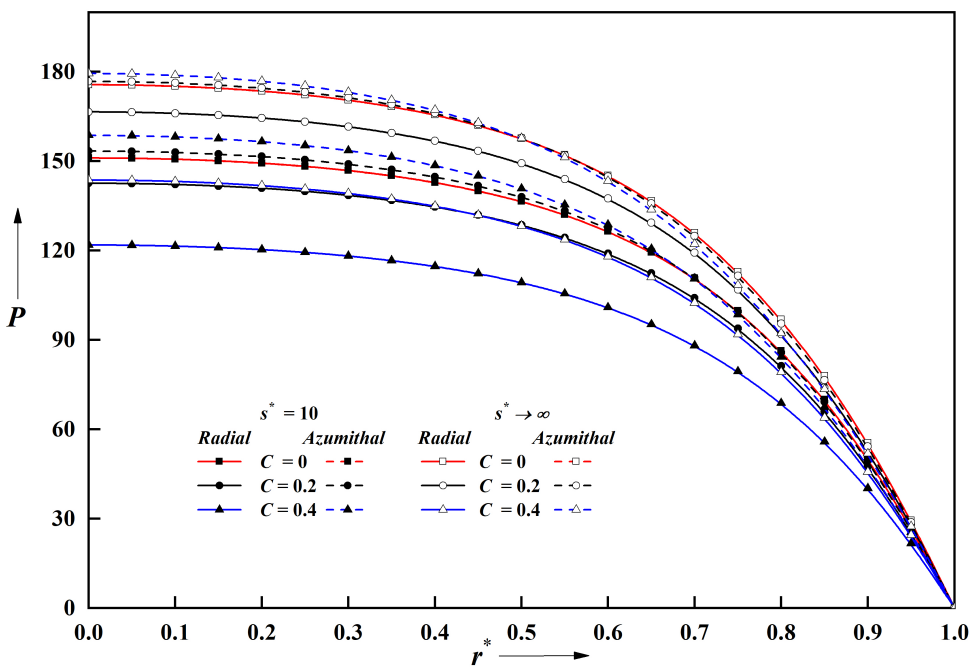

Figure 2: Figure 2: Dimensionless Pressure P^*against $r^*$with different C and fixed $M_0 = 2, l^* = 0.3$ and $\psi = 0.01$.

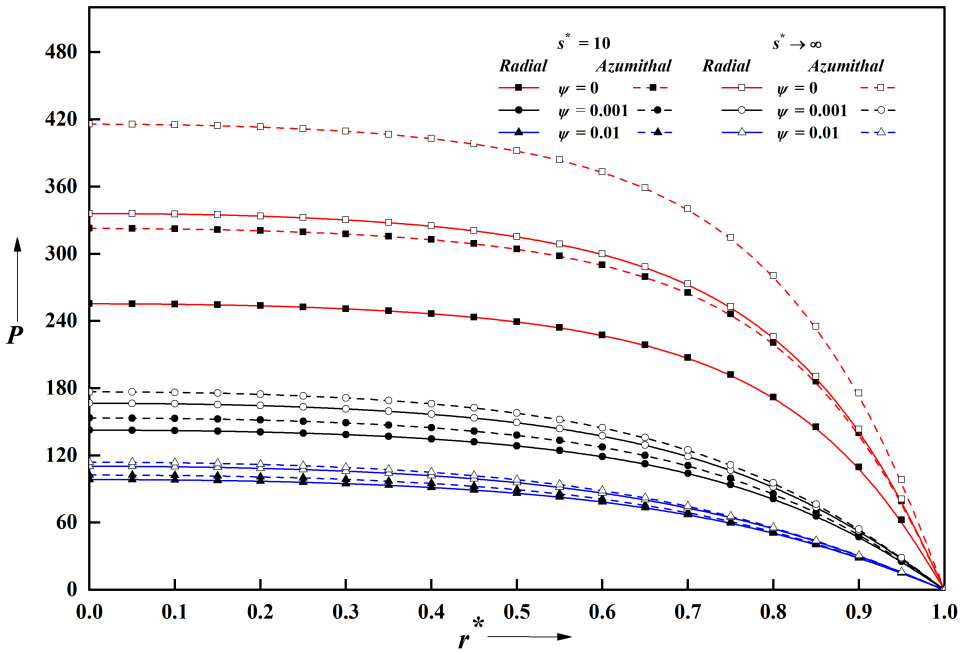

Figure 3: Variation of pressure P^* against r^* with different Ψ and fixed $M_0 = 2, l^* = 0.3$ and $C = 0.2$.

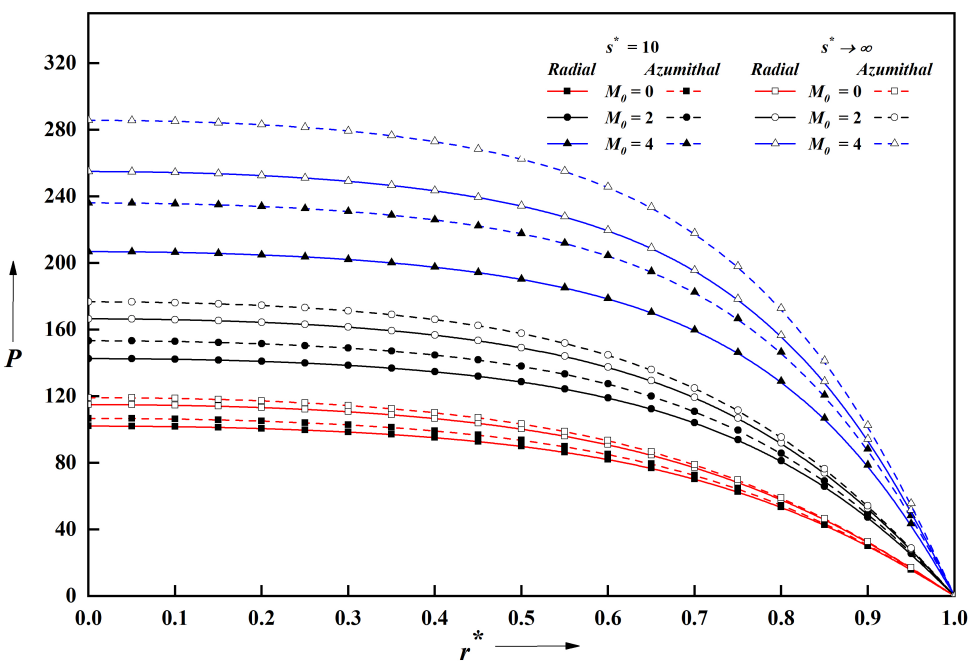

Figure 4: Variation of pressure P^* against r^* with different M_0 and fixed $\psi = 0.01, l^* = 0.3$ and $C = 0.2$.

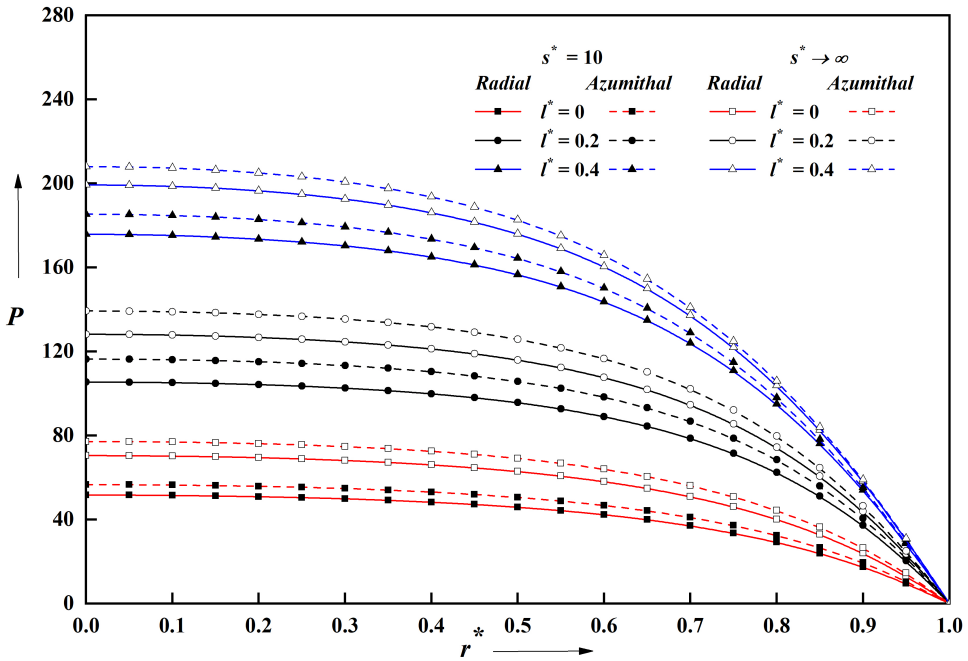

Figure 5: Variation of pressure P^* against r^* with different l^* and fixed $M_0 = 2, \psi = 0.01$ and $C = 0.2$.

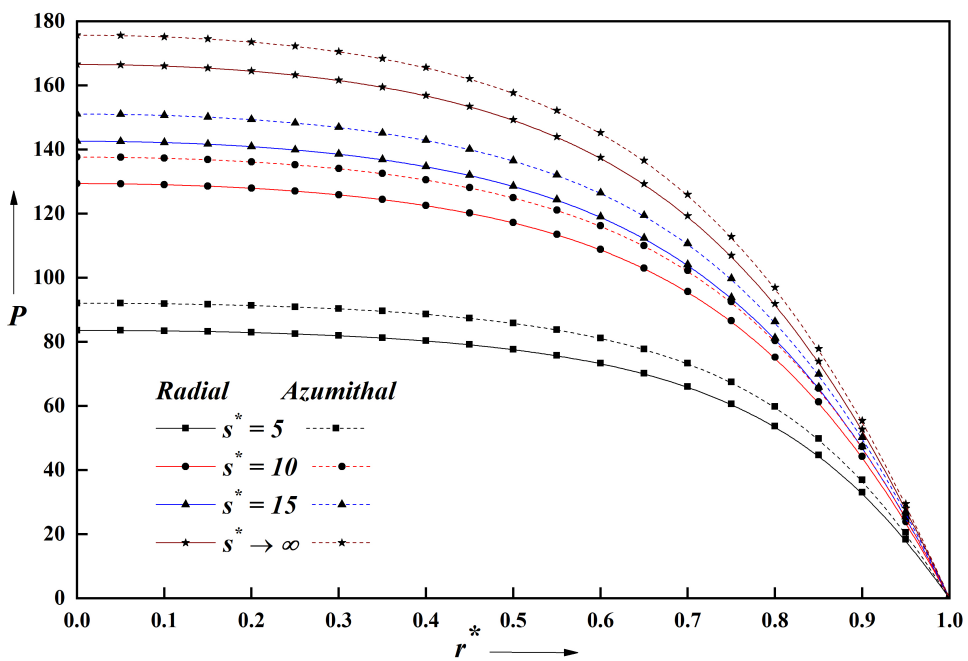

Figure 6: Variation of pressure P^* against r^* with different s^* and fixed $M_0 = 2, \psi = 0.01$ and $C = 0.2$.

3.2. Dimensionless Load Capacity

The graph of load bearing ability W^* versus β diverse values of C is elaborated in Figure 7 and found that the increase of roughness parameter the load capacity increases in the azimuthal roughness

pattern whereas it decreases in the radial roughness pattern. But load capacity is more significant in azimuthal rough surfaces. In Figure 8, Let W^* versus β for different ψ is portrayed, the result, mean load falloffs for increase of ψ values. The porousness allows fluid to escape from the porous area, which lowers the formation of film pressure and, consequently the load bearing capacity decreases. Figure 9 and 10 show the effects of M_0 and non-Newtonian lubricants on the load profile and seen that for increasing M_0 and couple stress lubricant enhances the load related to non-magnetic and Newtonian cases. Figure 11 explains how slip velocity affects the load profile the result indicates that the slip velocity parameter increases, which raises the load support.

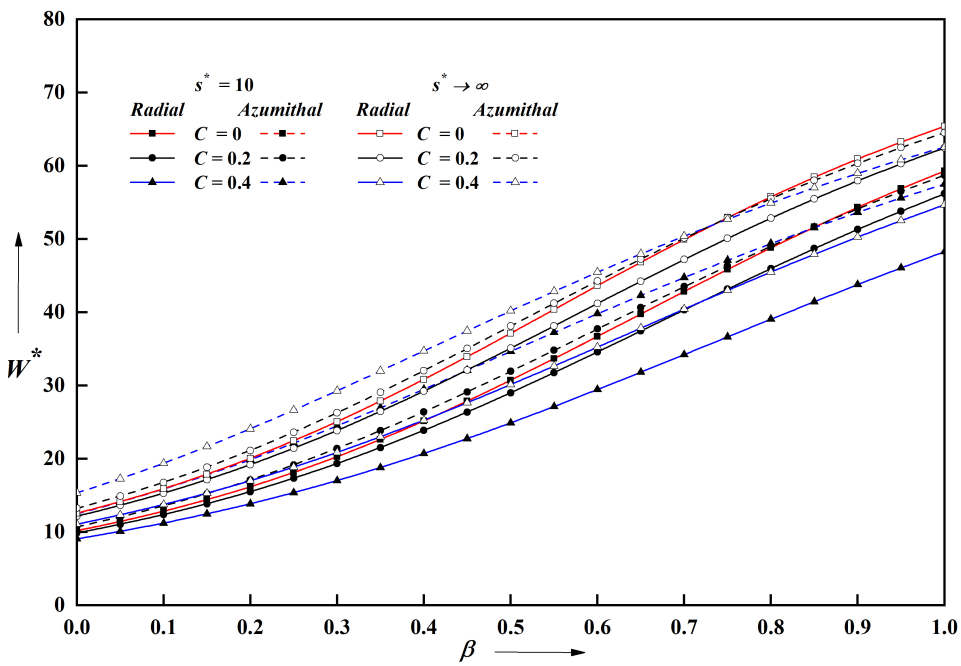

Figure 7: W^*against β with different C and fixed $M_0 = 2, l^* = 0.3$ and , $\psi = 0.01$.

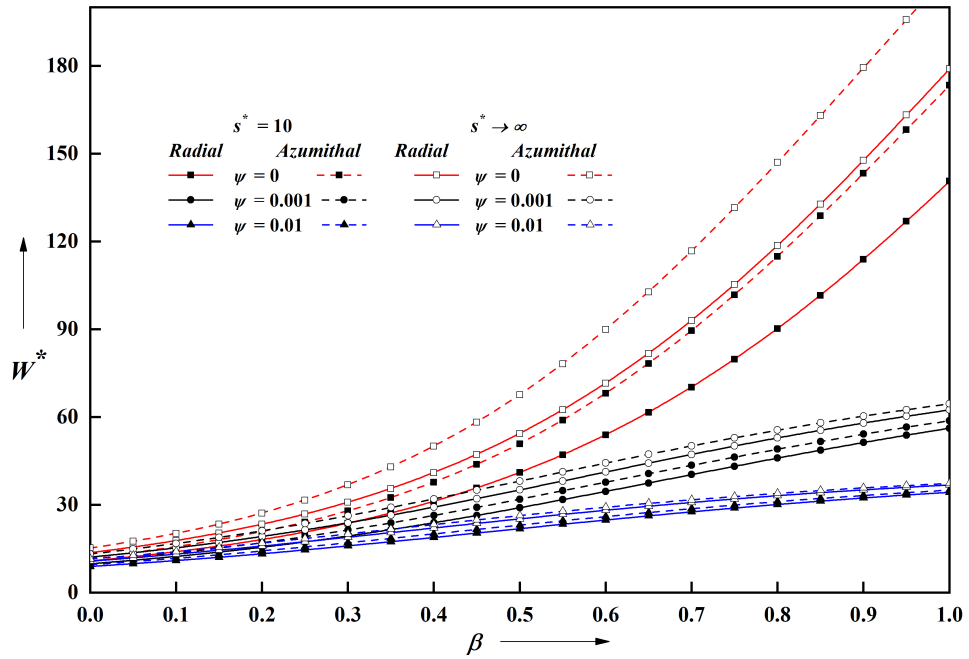

Figure 8: Variation of Load W^*against β with different ψ. and fixed $M_0 = 2, l^* = 0.3$ and $C = 0.2$.

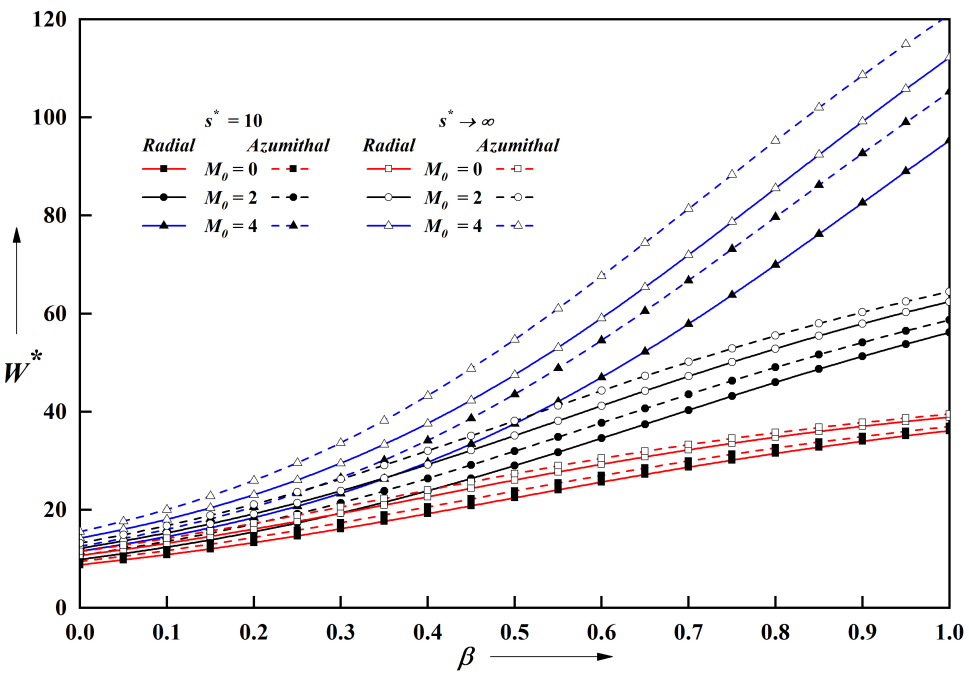

Figure 9: Variation of Load W^*against β with different M_0 and fixed $\psi = 0.01, l^* = 0.3$ and $C = 0.2$.

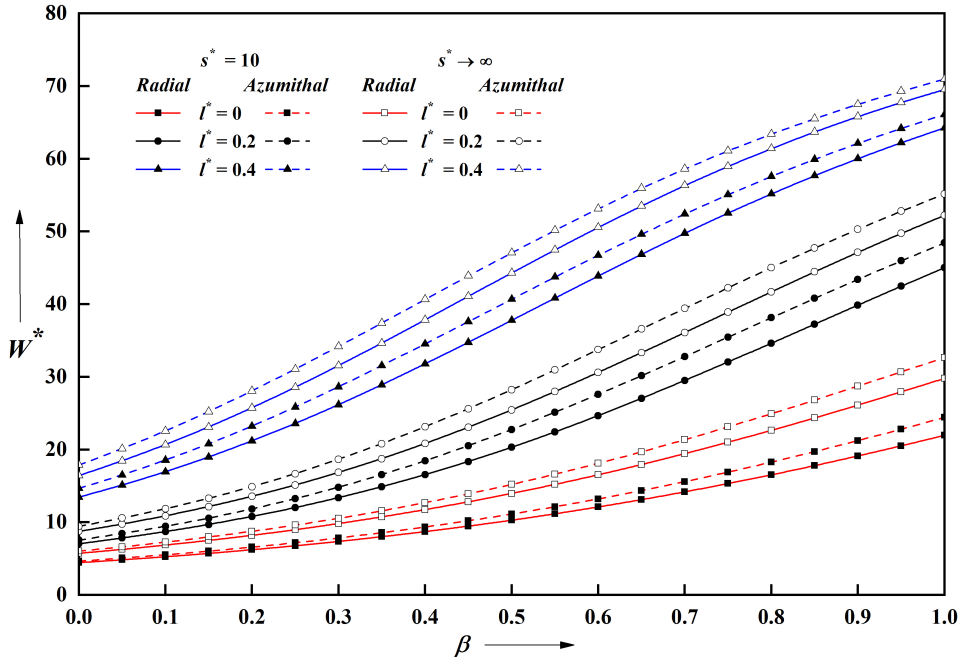

Figure 10: Variation of Load W^*against β with different l^* and fixed $M_0 = 2, \psi = 0.01$ and $C = 0.2$.

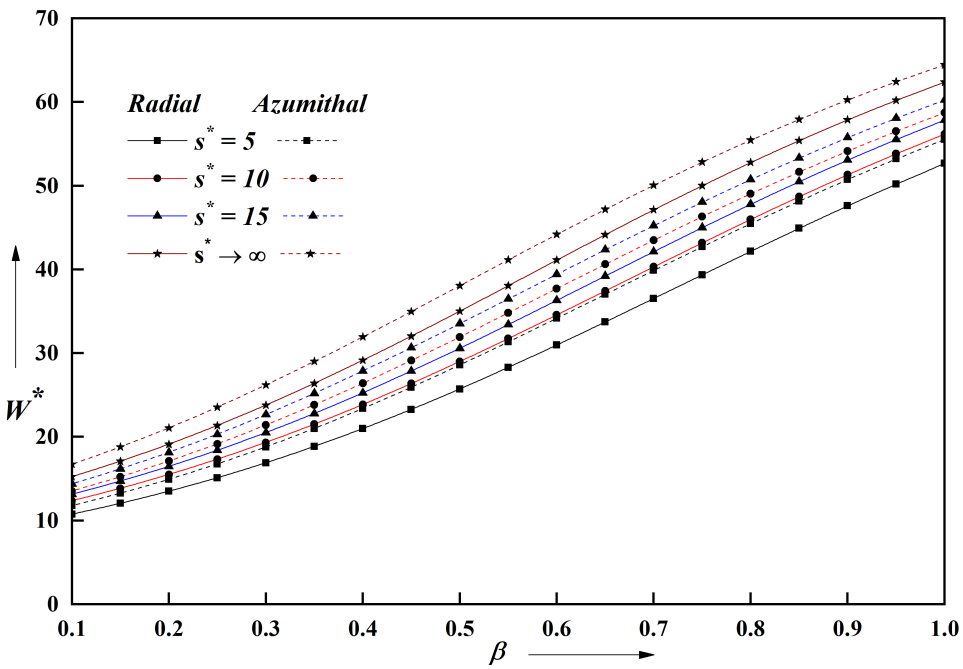

Figure 11: Variation of Load W^*against β with differents^* and fixed $M_0 = 2, l^* = 0.3.\psi = 0.01$ and $C = 0.2$.

3.3. Dimensionless Squeeze film time

Figure 12 illustrates the change in squeezing time T^* versus h_m^* for discrete values of C is illustrated for both roughness configurations. It is viewed that with the growing C values there is a considerable boost in T^*. The squeeze time of approach is additional expressive for patterns of azimuthal structure in comparison to the pattern of radial structure. In Figure 13, we plotted the squeeze film time T^* versus h_m^* for different ψ, which indicates that the lower the squeezing time for higher values of permeability parameter. Figure 14 and 15 displays dimensionless squeeze time T^* against h_m^* for diverse values of M_0 & l^*.We noticed that the M_0 & l^*enhances the squeeze film time on comparing with no-magnetic and Newtonian situation. Figure 16 demonstrates the impacts of slip velocity on squeeze film time and found that there is a larger of squeezing time for higher values of slip velocity.

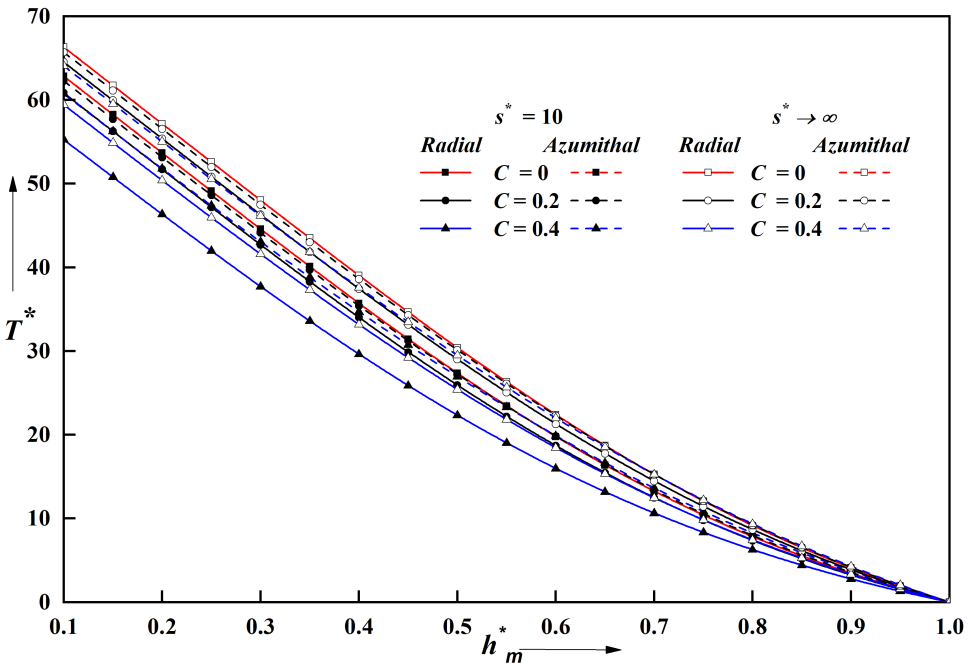

Figure 12: Dimensionless squeeze time T^*against $h_m^*$for different C and fixed $M_0 = 2, l^* = 0.3$ and $\psi = 0.01$.

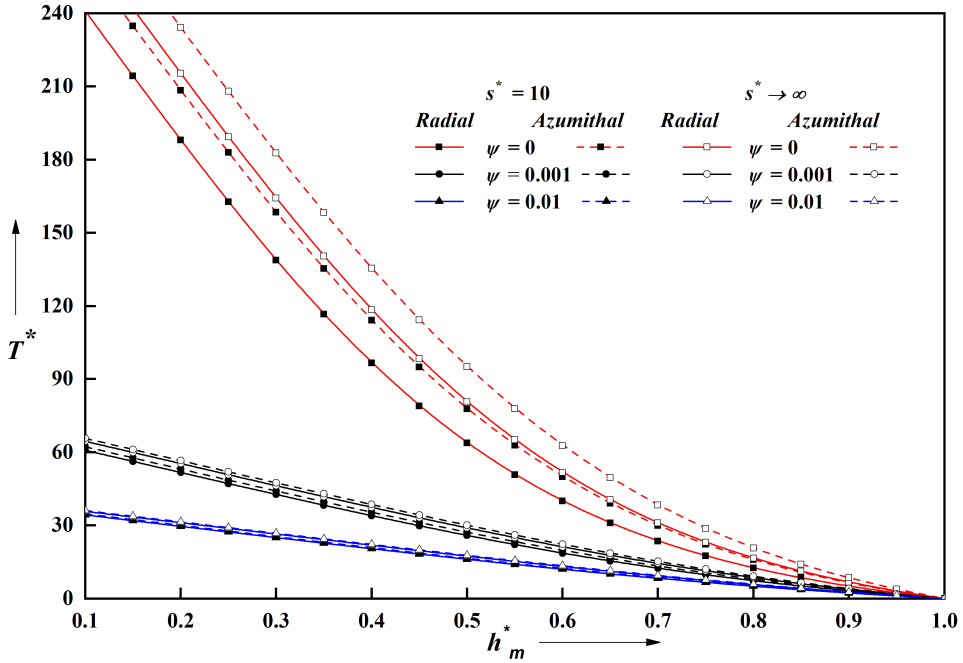

Figure 13: Dimensionless squeeze time T^* against $h_m^*$for different ψ and fixed $M_0 = 2, l^* = 0.3$ and $C = 0.2$.

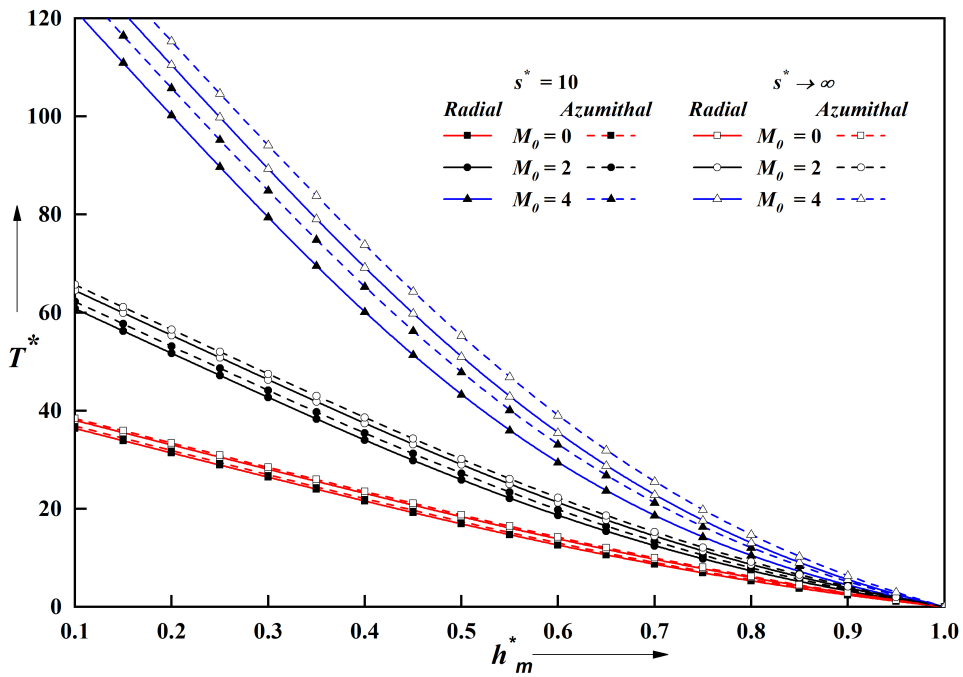

Figure 14: Dimensionless squeeze time T^* against h_m^* with different M and fixed $\psi = 0.01, l^* = 0.3$ and $C = 0.2$.

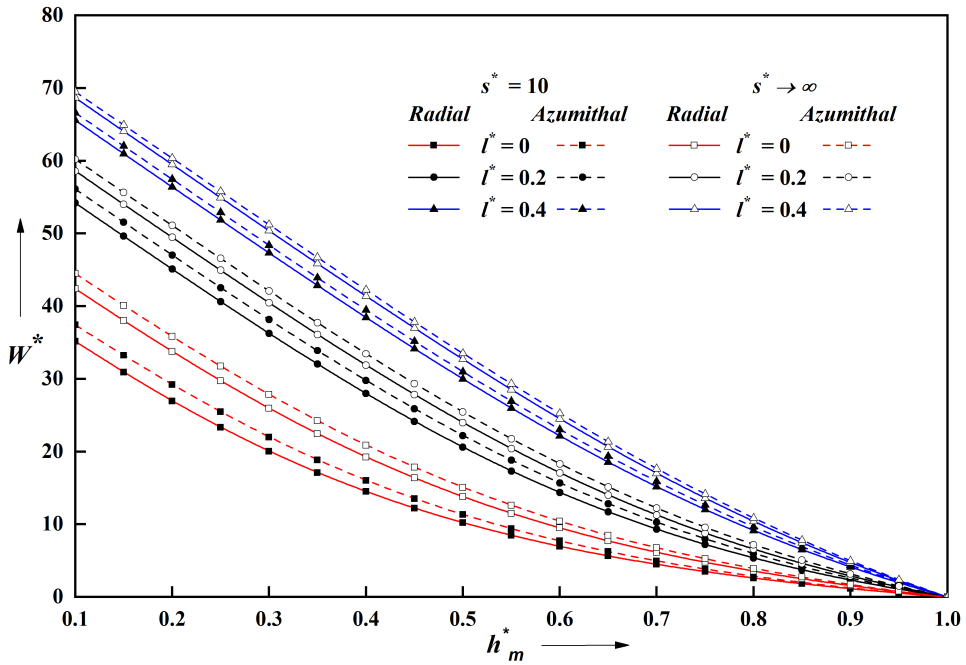

Figure 15: Dimensionless squeeze time T^* against h_m^* with l^* and fixed fixed $M_0 = 2, \psi = 0.01$ and $C = 0.2$.

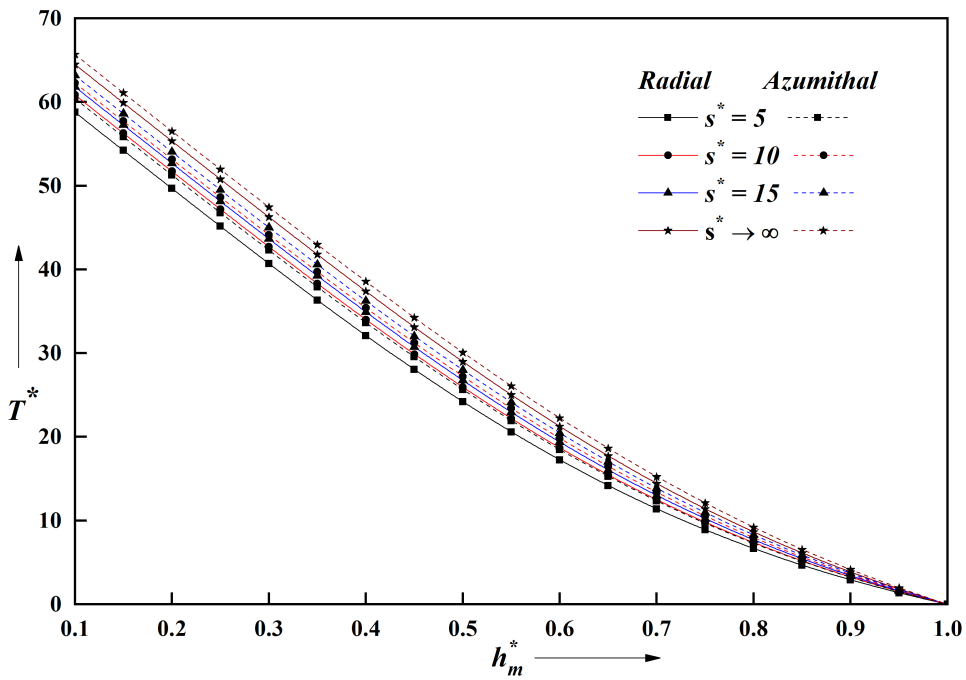

Figure 16: Dimensionless squeeze time T^* against h_m^* with s^* and fixed $M_0 = 2, l^* = 0.3, \psi = 0.01$ and $C = 0.2$.

4. Conclusion

The study explores the collective influence of MHD slip velocity and surface irregularities on the performance of a squeeze film containing couple-stress fluid between curved circular and flat plates. The examination is conducted using Christensen's theory for irregular (rough) surfaces and Darcy's law for porous structures. Based on this investigation, the following conclusions have been derived:

- A surface with roughness effects, compared to a smooth one, exhibits a longer squeeze film duration, greater load-supporting capacity, and higher pressure. Furthermore, azimuthal surface irregularities have a significantly stronger influence than radial roughness.
- The presence of a magnetic field, represented by the Hartmann number, enhances the squeezing characteristics of both roughness structures compared to non-magnetic conditions.
- The impression of couple stresses is more noticeable for azimuthal case, than for radial. When Newtonian dynamics is not applicable, the behaviour of the squeeze film becomes particularly important.
- The impact of permeability parameter reduces the pressure, squeezing time and load with growing values ϕ.
- As $\psi \to 0$, the squeeze-film attributes change to a non-permeable case.

Limiting Cases:

In the case of $C \to 0$ and $s \to 0$ also absence of porosity $\psi \to 0$, it corresponds to the smooth case discussed by Hiremath et al. [15]

References

1. Kuzma, D.C., *The magnetohydrodynamic journal bearing*. Journal of Basic Engineering 85(3), 424–427 (1963). https://doi.org/10.1115/1.3656630.
2. Krieger, R.J., Day, H.J., Hughes, W.F., *The MHD hydrostatic thrust bearing—Theory and experiments*. Journal of Tribology 89(3), 307–313 (1964). https://doi.org/10.1115/1.3616978.
3. Kamiyama, S., *Magnetohydrodynamic journal bearing (Report 1)*. Journal of Lubrication Technology 91(3), 380–386 (1969). https://doi.org/10.1115/1.3554944.
4. Malik, M., Singh, D.V., *Analysis of finite magnetohydrodynamic journal bearings*. Wear 64(2), 273–280 (1980). https://doi.org/10.1016/0043-1648(80)90133-7.
5. Lin, J.-R., *MHD steady and dynamic characteristics of wide tapered-land slider bearings*. Tribology International 43(12), 2378–2383 (2010). https://doi.org/10.1016/j.triboint.2010.07.010.
6. Lin, J.-R., *Effects of couple stresses on the lubrication of finite journal bearings*. Wear 206(1–2), 171–178 (1997). https://doi.org/10.1016/s0043-1648(96)07357-7.
7. Wang, X.-L., Zhu, K.-Q., Wen, S.-Z., *On the performance of dynamically loaded journal bearings lubricated with couple stress fluids*. Tribology International 35(3), 185–191 (2002). https://doi.org/10.1016/s0301-679x(01)00114-1.
8. Naduvinamani, N.B., Fathima, S.T., Hiremath, P.S., *Hydrodynamic lubrication of rough slider bearings with couple stress fluids*. Tribology International 36(12), 949–959 (2003). https://doi.org/10.1016/s0301-679x(03)00092-6.
9. Lin, J.R., Chu, L.M., Hung, C.R., Lu, R.F., *Magneto-hydrodynamic non-Newtonian curved circular squeeze film*. Journal of Marine Science and Technology 22(5), 566–571 (2014). https://doi.org/10.6119/JMST-013-0716-2.
10. Crosby, W.A., Chetti, B., *The static and dynamic characteristics of a two-lobe journal bearing lubricated with couple-stress fluid*. Tribology Transactions 52(2), 262–268 (2009). https://doi.org/10.1080/10402000802527773.
11. Chetti, B., Crosby, W.A., *Preload effects on the static characteristics of three-lobe journal bearings lubricated with a couple stress fluid*. Industrial Lubrication and Tribology 71(10), 1136–1143 (2019). https://doi.org/10.1108/ilt-12-2018-0435.
12. Biradar, K., Hanumagowda, B.N., *MHD effect on porous wide composite slider bearings lubricated with couple stress fluids*. Tribology Online 10(1), 11–20 (2015). https://doi.org/10.2474/trol.10.11.
13. Naduvinamani, N.B., Hosmani, S.S., *Porous exponential slider bearings lubricated with MHD-couple stress fluid*. Industrial Lubrication and Tribology 70(5), 838–845 (2018). https://doi.org/10.1108/ilt-03-2017-0057.
14. Patil, J., Hanumagowda, B.N., Neela, D., Patil, V., Ayyappa, G.H., Trimbak, V.B., Vijayalaxmi, P., *Analysis of MHD effects on porous flat plate and curved circular plate*. Journal of Advanced Research in Fluid Mechanics and Thermal Sciences 120(2), 82–98 (2024). https://doi.org/10.37934/arfmts.120.2.8298.

15. Ayyappa, G.H., Hanumagowda, B.N., Siddharam, P., Patil, J., *Influence of magnetic field on a curved circular plate and flat plate lubricated with non-Newtonian fluid*. Journal of Physics: Conference Series. https://doi.org/10.1088/1742-6596/1473/1/012011.

16. Devani, U., Patil, J., Bilal, S., Hanumagowda, B., Trimbak, V., Tawade, J., Nazarova, N., Gupta, M., *Study of MHD on porous flat and curved circular plate lubricated with couple stress fluid-A slip velocity model*. Results in Engineering (2024). https://doi.org/10.1016/j.rineng.2024.

17. Christensen, H., *Stochastic models for hydrodynamic lubrication of rough surfaces*. Proceedings of the Institution of Mechanical Engineers 184(1), 1013–1026 (1969). https://doi.org/10.1243/pime_proc_1969_184_07.

18. Gupta, J.L., Deheri, G.M., *Effect of roughness on the behavior of squeeze film in a spherical bearing*. Tribology Transactions 39(1), 99–102 (1996). https://doi.org/10.1080/10402009608983508.

19. Vijayalaxmi, P., Patil, J., Hanumagowda, B.N., Jagadish, T., Khan, I., *Performance of surface roughness of MHD slip velocity on curved circular and flat plates lubricated with non-Newtonian fluid*. International Journal of Hydrogen Energy 87(18), 1522–1532 (2024). https://doi.org/10.1016/j.ijhydene.2024.08.500.

20. Ramesh, S.K., Ayyappa, G.H., Patil, J., Hanumagowda, B.N., Mangala, K., Fateh, M.O., *Features of MHD on secant curved annular circular plate lubricant as a couple-stress fluid with slip velocity*. Journal of Advanced Research in Fluid Mechanics and Thermal Sciences 121(2), 201–215 (2024). https://doi.org/10.37934/arfmts.121.2.201215.

21. Ramesh, S.K., Ayyappa, G.H., Hanumagowda, B.N., Patil, J., Khan, I., *Influence of magneto-hydrodynamic and couple stress squeeze film lubrication on conical bearing-A slip velocity model*. Alexandria Engineering Journal 106, 735–742 (2024). https://doi.org/10.1016/j.aej.2024.08.064.

22. Jayaprakash, J., Vediyappan, G., Patil, J., Hanumagowda, B.N., Ahmed, H., Jagadish, V.T., *The effect of magneto-hydrodynamics on curved circular plate and porous-rough flat plate with non-Newtonian fluid*. Journal of Applied and Computational Mechanics 10(3), 584–596 (2024). https://doi.org/10.22055/jacm.2024.45684.4398.

23. Byeon, H., Latha, Y.L., Hanumagowda, B.N., Govindan, V., Salma, A., Abdullaev, S., Tawade, J.V., Awwad, F.A., Ismail, E.A.A., *Magnetohydrodynamics and viscosity variation in couple stress squeeze film lubrication between rough flat and curved circular plates*. Scientific Reports 13(1) (2023). https://doi.org/10.1038/s41598-023-50326-7.

24. Shah, R.C., *Ferrofluid lubrication of porous-rough circular squeeze film bearings*. European Physical Journal Plus 137(2) (2022). https://doi.org/10.1140/epjp/s13360-022-02344-z.

Shivaraj M. Dandoti,
Doddappa Appa PU Science College Kalaburagi, Karnataka, India.
E-mail address: shivarajmdandoti123@gmail.com

and

Jagadish Patil,
Department of Mathematics
Faculty of Engineering and Technology
Sharnbasva University
Kalaburagi,
Karnataka,
India.
E-mail address: jagadish_patil@sharnbasvauniversity.edu.in

and

Bannihalli Naganagowda Hanumagowda,
Department of Mathematics
School of Applied Sciences
REVA University
Bengaluru, Karnataka, India.
E-mail address: hanumagowda123@rediffmail.com

and

Suvarna Hindole,
Department of Mathematics

Poojya Doddappa Appa College of Engineering
Kalaburagi, Karnataka, India.
E-mail address: sshindole@pdaengg.com